3D Fourth-Order Staggered-Grid Finite-Difference Schemes: Stability and Grid Dispersion

by Peter Moczo, Jozef Kristek, and Ladislav Halada

Abstract   We investigated stability and grid dispersion in the 3D fourth-order in space, second-order in time, displacement-stress staggered-grid finite-difference scheme. Though only displacement-stress scheme is explicitly treated, all results also apply to the velocity-stress and displacement-velocity-stress finite-difference schemes.

We derived independent stability conditions for the *P* and *S* waves by exact separation of equations for the two types of waves.

Since the *S*-wave group velocity can differ from the actual velocity as much as 5% for the sampling ratio 1/5 (that is usually used in modeling), we recommend to sample a minimum *S* wavelength by six grid spacings.

Grid dispersion is strongest for a wave propagating in the direction of a coordinate axis and weakest for a wave propagating along a body diagonal.

Grid dispersion in the fourth-order scheme for the sampling ratios $s = 1/5$ and $s = 1/6$ is smaller than grid dispersion in the second-order scheme for $s = 1/10$ and $s = 1/12$, respectively.

Introduction

The staggered-grid finite-difference (FD) schemes became a very popular numerical tool for modeling seismic-wave propagation and earthquake ground motion after Virieux (1984, 1986) had presented his *SH* and *P-SV* second-order velocity-stress FD schemes. Levander (1988) applied the fourth-order approximation in space to the *P-SV* scheme. Luo and Schuster (1990) introduced the *P-SV* displacement-stress scheme and Olsen and Schuster (1992) extended it to the 3D case. Yomogida and Etgen (1993) used an approximate eighth-order displacement-stress scheme for the 3D modeling. Graves (1996) presented a 3D fourth-order velocity-stress scheme with effective material parameters. Ohminato and Chouet (1997) suggested a technique to include the free-surface topography in the 3D second-order displacement-stress modeling. Another technique to include the free-surface topography in the 3D velocity-stress modeling was suggested by Hestholm and Ruud (1998). Pitarka (1999) presented a 3D approximately fourth-order velocity-stress scheme on a rectangular grid with a varying size of a grid spacing. Aoi and Fujiwara (1999) applied a 3D second-order velocity-stress scheme on a discontinuous $h \times h \times h\_3h \times 3h \times 3h$ grid.

The staggered-grid FD schemes have been recently widely used for the 3D modeling of the earthquake ground motion, e.g., Graves (1993), Olsen *et al.* (1995), Pitarka *et al.* (1997, 1998), Cotton *et al.* (1998), Graves *et al.* (1998),

Matsushima *et al.* (1998), Wald and Graves (1998), and Kristek *et al.* (1999). The staggered-grid schemes have also been applied to seismic source and wave propagation modeling. However, as far as we know, stability and grid dispersion of the 3D staggered-grid schemes have not been sufficiently investigated. Dispersion curves were presented by Virieux (1986) and Levander (1988) for their velocity-stress 2D *P-SV* schemes. Crase *et al.* (1992) derived stability condition for the *P-SV* case of an arbitrary order of approximation using a decomposition of the matrix scheme and a Fourier transform.

Therefore, we focus in this article on the stability condition and grid dispersion in the 3D fourth-order in space, second-order in time, displacement-stress FD scheme. We present an exact derivation of the stability conditions for the *P* and *S* waves by strict separation of equations for the two types of waves. We obtain the grid-dispersion relations for both waves and use them for numerical investigation of the grid dispersion in space, coordinate-axis plane, body-diagonal plane, and three distinct directions of propagation. We also compare grid dispersion in the 3D fourth- and second-order schemes as well as the 3D and 2D *P-SV* schemes.

Though we explicitly treat the displacement-stress scheme, all results also apply to the velocity-stress and displacement-velocity-stress (Moczo *et al.,* in press) schemes.

Equation of Motion and the 3D Fourth-Order Displacement-Stress Finite-Difference Scheme

Consider Cartesian coordinate system (x, y, z). Let density ρ and Lamé elastic coefficients λ and μ be functions of spatial coordinates x, y, z. Let displacement vector $\bar{u}(u, v, w)$, stress tensor $\tau_{\varepsilon\kappa}$; $\varepsilon, \kappa \in \{x, y, z\}$, and body force per unit volume $\bar{f}$ (f_x, f_y, f_z) be functions of x, y, z and time t. The equation of motion and Hooke's law for a perfectly elastic, inhomogeneous, isotropic medium are

$$\rho u_{tt} = \tau_{xx,x} + \tau_{xy,y} + \tau_{xz,z} + f_x$$
$$\rho v_{tt} = \tau_{xy,x} + \tau_{yy,y} + \tau_{yz,z} + f_y \qquad (1a)$$
$$\rho w_{tt} = \tau_{xz,x} + \tau_{yz,y} + \tau_{zz,z} + f_z$$

and

$$\tau_{xx} = (\lambda + 2\mu)u_x + \lambda v_y + \lambda w_z$$
$$\tau_{yy} = \lambda u_x + (\lambda + 2\mu)v_y + \lambda w_z$$
$$\tau_{zz} = \lambda u_x + \lambda v_y + (\lambda + 2\mu)w_z \qquad (1b)$$
$$\tau_{xy} = \mu(u_y + v_x)$$
$$\tau_{xz} = \mu(u_z + w_x)$$
$$\tau_{yz} = \mu(v_z + w_y)$$

where $u_{tt} = \partial^2 u/\partial t^2$, $\tau_{xx,x} = \partial\tau_{xx}/\partial x$, $u_x = \partial u/\partial x$ and so on. We can call equations (1) the displacement-stress formulation of the equation of motion.

Consider a 3D regular rectangular staggered spatial grid with a grid spacing h. Denote Δt a time step and $a = -\frac{1}{24}$ and $b = \frac{9}{8}$ coefficients of the fourth-order approximation of the first derivative. Let $U^m_{I,K,L}$ be a discrete approximation to $u^m_{I,K,L} = u(x_I, y_K, z_L, t_m)$ where I, K, L are spatial indices and m is a time index. Similarly, let $V, W, T^{xx}, T^{yy}, T^{zz}, T^{xy}, T^{xz}, T^{yz}, F^x, F^y$, and F^z be discrete approximations to $v, w, \tau_{xx}, \tau_{yy}, \tau_{zz}, \tau_{xy}, \tau_{xz}, \tau_{yz}, f_x, f_y$, and f_z. For equations (1) we can construct an explicit fourth-order in space, second-order in time, displacement-stress staggered-grid FD scheme. The scheme is given in the Appendix.

Stability Condition for an Unbounded Homogenous Medium

To analyze stability of the FD scheme we use the von Neumann (1943) method that assumes harmonic decomposition of the errors at a given time. Assume errors in $U, V, W, T^{xx}, T^{yy}, T^{zz}, T^{xy}, T^{xz}$, and T^{yz} at $x = Ih$, $y = Kh$, $z = Lh$, and $t = m\Delta t$ in the form

$$e(U) = AE, \quad e(V) = BE, \quad e(W) = CE$$
$$e(T^{xx}) = D_1 E, \quad e(T^{yy}) = D_2 E, \quad e(T^{zz}) = D_3 E \qquad (2)$$
$$e(T^{xy}) = D_4 E, \quad e(T^{xz}) = D_5 E, \quad e(T^{yz}) = D_6 E$$

$$E = \exp i(-\omega m \Delta t + k_x Ih + k_y Kh + k_z Lh)$$

where ω is an angular frequency, k_x, k_y, and k_z are the components of the wavenumber vector $\bar{k}$,

$$k_x = k \cos \varphi \sin \delta, \quad k_y = k \sin \varphi \sin \delta,$$
$$k_z = k \cos \delta, \quad k = |\bar{k}| \qquad (3)$$

and angles δ and ϕ (illustrated in Fig. 1) are from intervals

$$0 \le \delta \le \pi \qquad 0 \le \varphi \le 2\pi.$$

Investigate propagation of the errors (2) in the grid. Inserting (2) into the FD scheme (see appendix) leads to the system of equations

$$\begin{bmatrix} A \\ B \\ C \end{bmatrix} \gamma = \begin{bmatrix} \xi^2 X^2 + \beta^2 \Sigma & \xi^2 XY & \xi^2 XZ \\ \xi^2 XY & \xi^2 Y^2 + \beta^2 \Sigma & \xi^2 YZ \\ \xi^2 XZ & \xi^2 YZ & \xi^2 Z^2 + \beta^2 \Sigma \end{bmatrix} \begin{bmatrix} A \\ B \\ C \end{bmatrix} \qquad (4)$$

where

$$\gamma = \frac{S^2}{\Delta^2}, \qquad S = \sin\tfrac{1}{2}\omega\Delta t, \qquad \Delta = \frac{\Delta t}{h}$$
$$\xi^2 = \frac{\lambda + \mu}{\rho}, \qquad \beta^2 = \frac{\mu}{\rho}$$

β being the S-wave velocity,
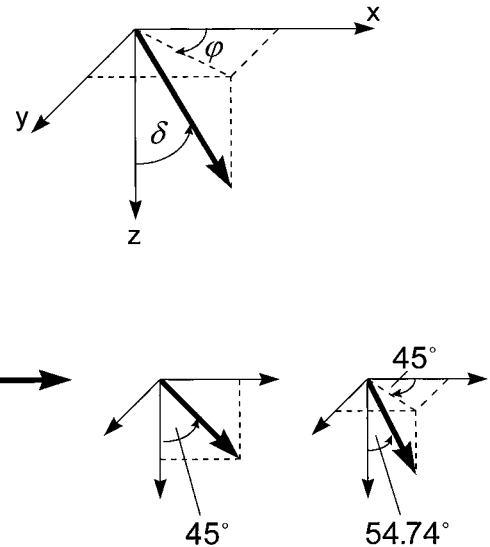
Figure 1. The Cartesian coordinate system and angles δ and φ that determine a direction of propagation. Three distinct directions of propagation investigated in the study: along a coordinate axis, coordinate-plane diagonal, and body diagonal.

$$X = a \sin k_x \tfrac{3}{2} h + b \sin k_x \tfrac{1}{2} h$$

$$Y = a \sin k_y \tfrac{3}{2} h + b \sin k_y \tfrac{1}{2} h \qquad (5)$$

$$Z = a \sin k_z \tfrac{3}{2} h + b \sin k_z \tfrac{1}{2} h$$

and

$$\Sigma = X^2 + Y^2 + Z^2.$$

Denoting the matrix in equation (4) by **M** and rearranging the equation we have

$$[\mathbf{M} - \gamma \mathbf{1}] \begin{bmatrix} A \\ B \\ C \end{bmatrix} = \begin{bmatrix} 0 \\ 0 \\ 0 \end{bmatrix}$$

where **1** is a unit matrix. A nontrivial solution exists if

$$Det[\mathbf{M} - \gamma \mathbf{1}] = 0. \qquad (6)$$

Rewrite the matrix:

$$[\mathbf{M} - \gamma \mathbf{1}] = \xi^2 \left[\begin{bmatrix} X & & \\ & Y & \\ & & Z \end{bmatrix} \begin{bmatrix} 1 & 1 & 1 \\ 1 & 1 & 1 \\ 1 & 1 & 1 \end{bmatrix} \begin{bmatrix} X & & \\ & Y & \\ & & Z \end{bmatrix} + d\mathbf{1} \right]$$

where

$$d = \frac{\beta^2 \, \Sigma - \gamma}{\xi^2}.$$

Then equation (6) can be rewritten as

$$\xi^6 \, Det \left[\begin{bmatrix} X & & \\ & Y & \\ & & Z \end{bmatrix} \begin{bmatrix} 1 & 1 & 1 \\ 1 & 1 & 1 \\ 1 & 1 & 1 \end{bmatrix} \begin{bmatrix} X & & \\ & Y & \\ & & Z \end{bmatrix} + d\mathbf{1} \right] = 0$$

and

$$Det \begin{bmatrix} X^2 + d & XY & XZ \\ XY & Y^2 + d & YZ \\ XZ & YZ & Z^2 + d \end{bmatrix} = 0$$

from which we obtain

$$d^2(X^2 + Y^2 + Z^2 + d) = 0. \qquad (7)$$

Equation (7) is satisfied if

$$X^2 + Y^2 + Z^2 + d = 0 \qquad (8)$$

or

$$d = 0. \qquad (9)$$

From equations (8) and (9) we obtain, respectively,

$$S^2 = \Delta^2 \, \alpha^2 (X^2 + Y^2 + Z^2)$$
$$S^2 = \Delta^2 \, \beta^2 (X^2 + Y^2 + Z^2)$$

from which we finally have

$$\sin \tfrac{1}{2} \omega \, \Delta t = \pm \frac{\Delta t}{h} \alpha (X^2 + Y^2 + Z^2)^{1/2} \qquad (10)$$

$$\sin \tfrac{1}{2} \omega \, \Delta t = \pm \frac{\Delta t}{h} \beta (X^2 + Y^2 + Z^2)^{1/2} \qquad (11)$$

where α is the *P*-wave velocity,

$$\alpha^2 = \frac{\lambda + 2\mu}{\rho}$$

and *X*, *Y*, *Z* are given by equations (5). Thus, we obtained two independent equations: equation (10) for the *P* wave and equation (11) for the *S* wave. Equation (10) implies a stability condition for the *P* wave:

$$\Delta t \leq \frac{6}{7\sqrt{3}} \frac{h}{\alpha} \qquad (12)$$

Similarly, equation (11) implies a stability condition for the *S* wave:

$$\Delta t \leq \frac{6}{7\sqrt{3}} \frac{h}{\beta}$$

If both types of waves are generated and propagate in a medium, condition (12) for the *P* wave has to be taken as the joint stability condition since $\alpha > \beta$.

Later we will use a stability parameter *p*, which can be defined as

$$p = \frac{7\sqrt{3}}{6} \frac{\Delta t}{h} \alpha, \qquad (13)$$

which means that

$$p \leq 1.$$

Grid Dispersion

Both equations (10) and (11) can be (omitting the minus sign) rewritten in the form

$$\frac{1}{2} \omega \Delta t = \arcsin \left[\frac{\Delta t}{h} c(X^2 + Y^2 + Z^2)^{1/2} \right] \quad (14)$$

where c is either the P-wave velocity α or S-wave velocity β for the P or S wave, respectively. Since ω is the angular frequency in the grid,

$$\omega = 2\pi \frac{c^{\mathrm{grid}}}{\lambda^{\mathrm{grid}}} \quad (15)$$

where c^{grid} and λ^{grid} are the phase velocity and wavelength in the grid, equation (14) represents grid-dispersion relations for the P and S waves propagating in the grid.

Define a spatial sampling ratio s for the S wave at a given frequency as

$$s = \frac{h}{\lambda_S^{\mathrm{grid}}} \quad (16)$$

Similarly, we can define a spatial sampling ratio s_P for the P wave at a given frequency as

$$s_P = \frac{h}{\lambda_P^{\mathrm{grid}}}.$$

However, if both types of waves are generated and propagate in a medium we have to adopt one joint spatial sampling ratio in order to compare the P- and S-wave dispersion. Since, at a given frequency, the S wave has a shorter wavelength, the spatial sampling ratio for the S wave has to be taken as an argument in relations for both the P and S waves. Obviously, a spatial sampling ratio s_P for the P wave relates to that for the S wave as

$$s_P = \frac{s}{r} \quad (17)$$

where r is a velocity ratio

$$r = \frac{\alpha}{\beta}. \quad (18)$$

Dividing equation (14) for the P wave and S wave by α and β, respectively, and inserting relations (3, 5, 15–18) we obtain the normalized grid-dispersion relations for the P and S waves in the form

$$\frac{\alpha^{\mathrm{grid}}}{\alpha} = q \frac{\sqrt{3}}{\pi} \frac{r}{p \cdot s} \arcsin \left(\frac{1}{q\sqrt{3}} p F_{\alpha} \right) \quad (19)$$

$$\frac{\beta^{\mathrm{grid}}}{\beta} = q \frac{\sqrt{3}}{\pi} \frac{r}{p \cdot s} \arcsin \left(\frac{1}{q\sqrt{3}} \frac{p}{r} F_{\beta} \right) \quad (20)$$

where

$$q = \frac{7}{6}$$

$$F_{\eta} = \{ [a \sin (3\pi\varsigma \cos \varphi \sin \delta) + b \sin (\pi\varsigma \cos \varphi \sin \delta)]^2$$
$$+ [a \sin (3\pi\varsigma \sin \varphi \sin \delta) + b \sin (\pi\varsigma \sin \varphi \sin \delta)]^2$$
$$+ [a \sin (3\pi\varsigma \quad \cos \delta) + b \sin (\pi\varsigma \quad \cos \delta)]^2 \}^{1/2}$$

p, s, and r are given by equations (13), (16), and (18), and

$$\varsigma = \frac{s}{r} \quad \text{if} \quad \eta = \alpha$$

or

$$\varsigma = s \quad \text{if} \quad \eta = \beta.$$

Note that both the P- and S-wave grid dispersions depend now on the velocity ratio $r = \frac{\alpha}{\beta}$ (and thus on the Poisson's ratio $\sigma = (2 - r^2)/[2(1 - r^2)])$. The dependence of the S-wave dispersion on the velocity ratio r was introduced by considering the P-wave stability condition (12) as a joint condition for both the P and S waves. The dependence of the P-wave dispersion on the velocity ratio r was introduced by considering the spatial sampling ratio for the S wave, $s = h/\lambda_s^{\mathrm{gnid}}$, as a joint argument in the dispersion relations (19) and (20) for both types of waves.

Let us note that the grid-dispersion relations in the case of the second-order scheme are obtained from relations (19) and (20) by inserting $a = 0$, $b = 1$, and $q = 1$. A stability parameter p in the second-order scheme is defined as

$$p = \sqrt{3} \frac{\Delta t}{h} \alpha, \qquad p \leq 1.$$

For completeness, the dispersion relations in the 2D P-SV case are given in the appendix.

The existence of the grid dispersion of the phase velocity implies the existence of the grid group velocity $c_{\mathrm{group}}^{\mathrm{grid}} = \partial\omega/\partial k$ and its dispersion. We easily obtain

$$\frac{\alpha_{\mathrm{group}}^{\mathrm{grid}}}{\alpha} = \frac{2(f_1\Gamma_1 + f_2\Gamma_2 + f_3\Gamma_3)}{\left[F - \left(\frac{6}{7\sqrt{3}} pF \right)^2 \right]^{1/2}}$$

$$\frac{\beta_{\mathrm{group}}^{\mathrm{grid}}}{\beta} = \frac{2(f_1\Gamma_1 + f_2\Gamma_2 + f_3\Gamma_3)}{\left[F - \left(\frac{6}{7\sqrt{3}} \frac{p}{r} F \right)^2 \right]^{1/2}}$$

where

$$f_1 = a \sin (3\pi\varsigma \cos \varphi \sin \delta) + b \sin (\pi\varsigma \cos \varphi \sin \delta)$$

$$f_2 = a \sin (3\pi\varsigma \sin \varphi \sin \delta) + b \sin (\pi\varsigma \sin \varphi \sin \delta)$$

$$f_3 = a \sin (3\pi\varsigma \quad \cos \delta) + b \sin (\pi\varsigma \quad \cos \delta)$$

$$\Gamma_1 = \cos \varphi \sin \delta \left[a \frac{3}{2} \cos (3\pi\varsigma \cos \varphi \sin \delta) \right.$$

$$\left. + b \frac{1}{2} \cos (\pi\varsigma \cos \varphi \sin \delta) \right]$$

$$\Gamma_2 = \sin \varphi \sin \delta \left[a \frac{3}{2} \cos (3\pi\varsigma \sin \varphi \sin \delta) \right.$$

$$\left. + b \frac{1}{2} \cos (\pi\varsigma \sin \varphi \sin \delta) \right]$$

$$\Gamma_3 = \cos \delta \left[a \frac{3}{2} \cos (3\pi\varsigma \quad \cos \delta) \right.$$

$$\left. + b \frac{1}{2} \cos (\pi\varsigma \quad \cos \delta) \right]$$

$$F = f_1^2 + f_2^2 + f_3^2$$

and

$$\varsigma = \frac{s}{r} \text{ in the case of } \frac{\alpha_{\text{group}}^{\text{grid}}}{\alpha} \text{ or } \varsigma = s \text{ in the case } \frac{\beta_{\text{group}}^{\text{grid}}}{\beta}.$$

Grid Dispersion: Numerical Results

Propagation in Space

In order to investigate the grid dispersion in space, let us define the following set of directions of propagation:

$$(\varphi, \delta) \in \Phi_1 \times \Delta_1 \cup \Phi_2 \times \Delta_2 \qquad (21)$$

Here, ϕ and δ are angles shown in Figure 1 and

$$\Phi_1 = \{0°\}$$
$$\Phi_2 = \{0°, 5°, 10°, 15°, \ldots, 40°, 45°\}$$
$$\Delta_1 = \{45°, 50°, 54.74°, 55°, 60°, \ldots, 85°, 90°\}$$
$$\Delta_2 = \{5°, 10°, \ldots, 45°, 50°, 54.74°, 55°, 60°, \ldots, 80°, 85°\}.$$

Set (21) determines 173 directions of propagation in total. We checked that this set is sufficient to show scatter of the dispersion curves for different possible directions of propagation in space. Figure 2(a) shows dispersion curves for the *P* wave for three values of the Poisson's ratio σ and three values of the stability parameter *p*. Analogously, Figure 3(a) shows dispersion curves for the *S* wave. Two vertical lines shown for each set of the curves indicate two values of the spatial sampling ratio, $s = 1/6$ and $s = 1/5$, that are used by seismologists in numerical simulations.

Obviously, it is desirable to run any computation in a homogeneous medium at a stability limit ($p = 1.0$), i.e., with the maximum possible value of the time step, since a smaller value of the time step would increase a total computational time. There is, however, a very important reason to show dispersion also for *p* as low as 0.5 and 0.1 that mean one-half and one-tenth of the maximum time step, respectively. One usually simulates a wave propagation in a model consisting of several homogeneous layers and/or blocks. In seismic ground motion simulation it is usual to have model with a (minimum *P*-wave velocity in sediments/maximum *P*-wave velocity in bedrock) ratio of 2 and more, sometimes even 10. Since the time step is determined according to a medium with the largest velocity, it is 2 to 10 times smaller than that required by the medium with the minimum velocity. Correspondingly, an effective stability ratio for a medium with the minimum velocity is as low as 0.5 to 0.1.

As expected, due to a longer wavelength of the *P* wave at the same frequency, propagation of the *P* wave is modeled by the FD scheme much better than that of the *S* wave. Compared to the *P* wave, there is relatively considerable grid-dispersion anisotropy of the *S* wave.

For a given Poisson's ratio σ and direction of propagation, both $\alpha^{\text{grid}}/\alpha$ and $\beta^{\text{grid}}/\beta$ decrease with a decreasing value of the stability parameter *p*. Sensitivity of $\beta^{\text{grid}}/\beta$ to the stability parameter *p* decreases with an increasing value of the Poisson's ratio σ. For a given direction of propagation and stability parameter *p*, $\beta^{\text{grid}}/\beta$ decreases with an increasing Poisson's ratio σ.

For a given direction of propagation, the *S*-wave dispersion curves for all values of the Poisson's ratio σ are very close to each other in the case of the stability parameter $p = 0.1$. This is understandable if we examine a limit of $\beta^{\text{grid}}/\beta$ for $p \to 0$. According to relation (20)

$$\beta^{\text{grid}}/\beta = \psi \frac{r}{p} \arcsin \left(\chi \frac{p}{r} \right)$$

where the meaning of $\psi = \psi(s)$ and $\chi = \chi(s, \delta, \phi)$ is clear from relation (20). It is easy to find that

$$\lim_{p \to 0} (\beta^{\text{grid}}/\beta) = \psi \cdot \chi.$$

This explains why the dispersion curves (for a given direction of propagation) for *p* as low as 0.1 are so close to each other regardless of the value of the Poisson's ratio σ.

Majority of the displayed *S*-wave dispersion curves exhibit $\beta^{\text{grid}}/\beta < 1$. Thus, in majority cases, the grid dispersion causes delays of the *S*-wave arrivals. There are, however, some curves that exhibit $\beta^{\text{grid}}/\beta > 1$ at certain intervals of the sampling ratio *s*.

Table 1 shows minimum β^{grid} in percentage of β for two values of the sampling ratio *s*, $s = 1/5$ and $s = 1/6$, three values of the Poisson's ratio σ and three values of the stability parameter *p*. It is clear from Table 1 that for $s = 1/5$ and $s = 1/6$, β^{grid} does not differ from the actual velocity β more than, approximately, 1% and 0.5%, respectively. Consider,

GRID DISPERSION FOR P WAVE, 4th-ORDER 3D DISPLACEMENT-STRESS

(a)

GRID DISPERSION FOR P WAVE, 4th-ORDER 3D DISPLACEMENT-STRESS

(b)
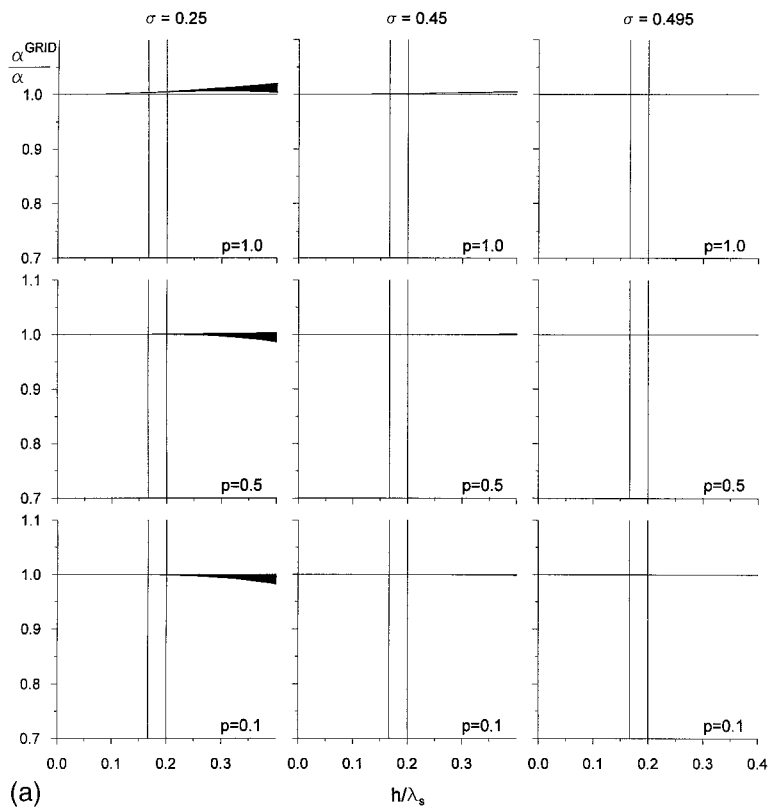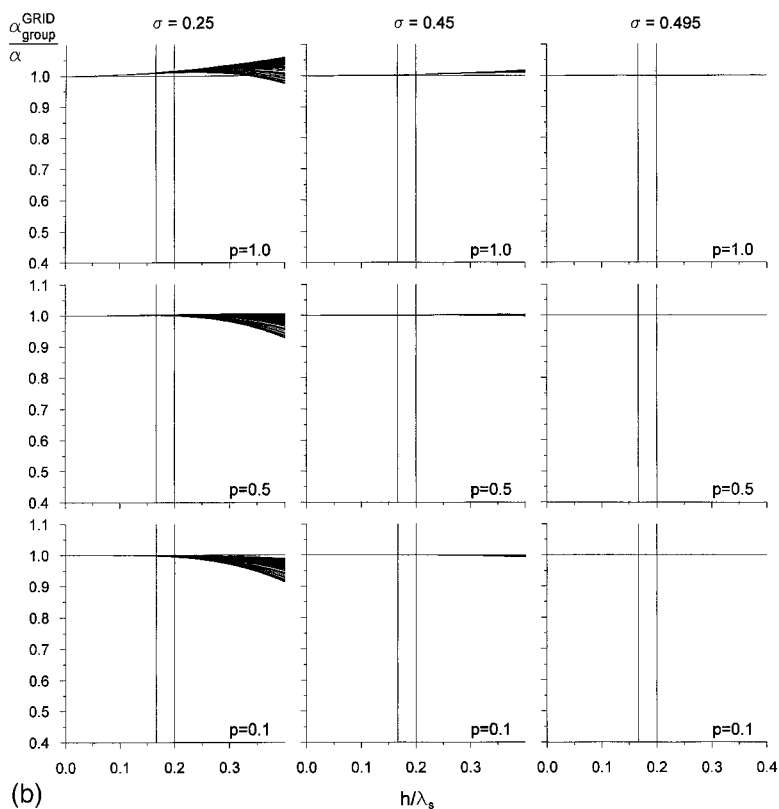
Figure 2. (a) Grid-dispersion curves for the P wave propagating in 173 directions in space. The set of directions is sufficient to show scatter of dispersion curves for all possible directions of propagation in space. Dispersion curves are shown for three values of the Poisson's ratio σ and three values of the stability parameter p. The three values of σ, 0.25, 0.45, and 0.495, correspond to α/β ratios of $\sqrt{3}$, 3.317, and 10, respectively. Two vertical lines indicate two values of the spatial sampling ratio ($s = h/\lambda_S$), $s = 1/6$ and $s = 1/5$, that are used by seismologists in numerical simulations. The horizontal line $\alpha^{grid}/\alpha = 1$ indicating the case of no grid dispersion is also shown for convenience. (b) The same as in Figure 2(a) but for the group velocity.

GRID DISPERSION FOR S WAVE, 4th-ORDER 3D DISPLACEMENT-STRESS

(a)

GRID DISPERSION FOR S WAVE, 4th-ORDER 3D DISPLACEMENT-STRESS

(b)
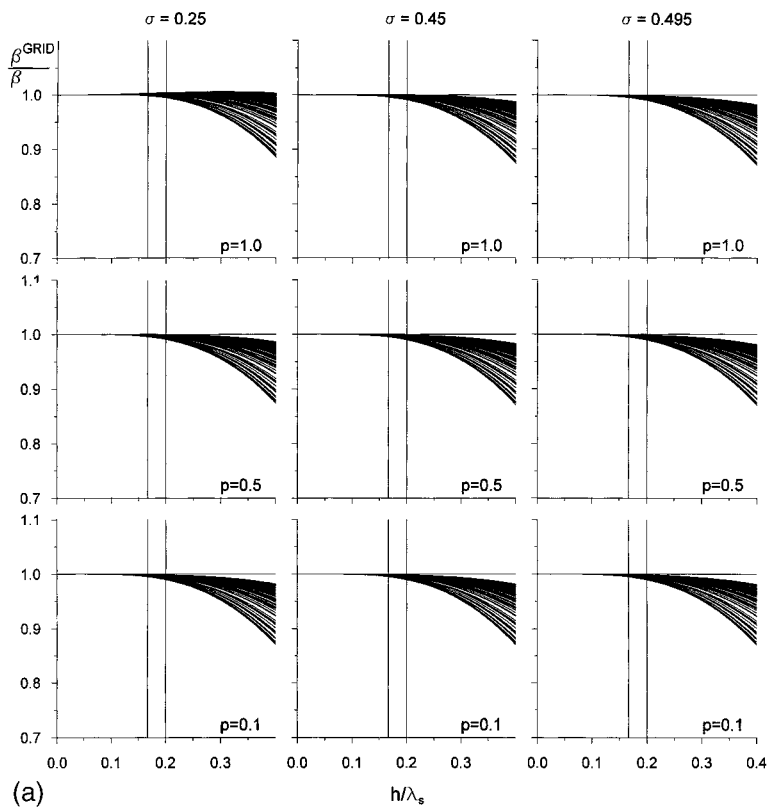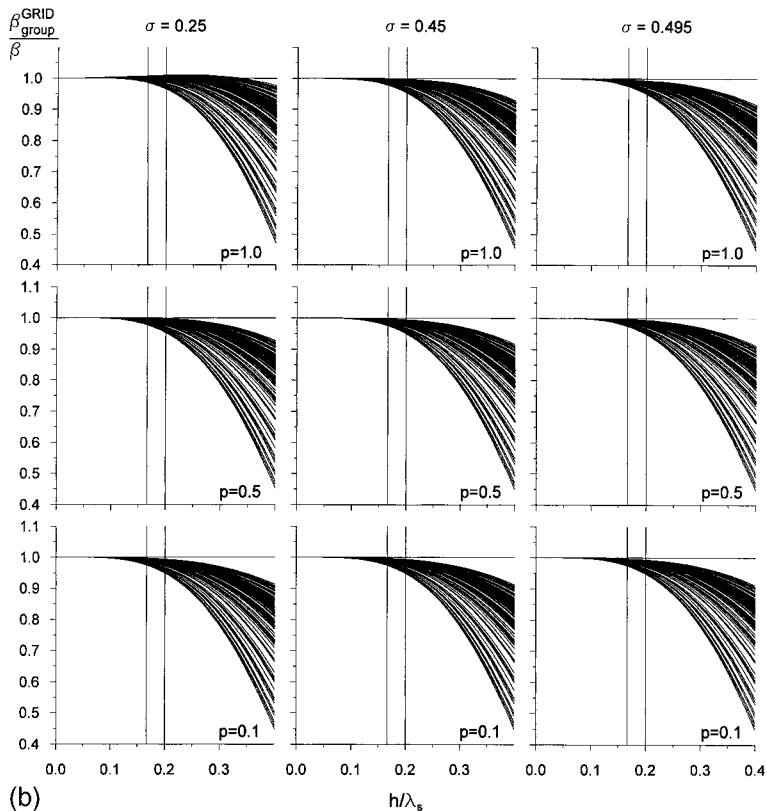
Figure 3. (a) Grid-dispersion curves for the *S* wave propagating in 173 directions in space. Compare with Figure 2(a) for the *P* wave. (b) The same as in Figure 3(a) but for the group velocity.

Table 1
Minimum Grid S-Wave Phase Velocities β^{grid} in % of the
Actual Velocity β

	$s = 1/5$		
	σ		
p	0.25	0.45	0.495
1.0	99.463	99.078	98.951
0.5	99.066	98.971	98.940
0.1	98.941	98.937	98.936
	$s = 1/6$		
	σ		
p	0.25	0.45	0.495
1.0	99.843	99.572	99.483
0.5	99.564	99.497	99.475
0.1	99.476	99.473	99.472

s, spatial sampling ratio; σ, Poisson's ratio; p, stability parameter.

Table 2
Minimum Grid S-Wave Group Velocities $\beta^{\mathrm{grid}}_{\mathrm{group}}$ in % of the
Actual Velocity β

	$s = 1/5$		
	σ		
p	0.25	0.45	0.495
1.0	96.410	95.288	94.922
0.5	95.253	94.979	94.888
0.1	94.892	94.881	94.878
	$s = 1/6$		
	σ		
p	0.25	0.45	0.495
1.0	98.525	97.723	97.460
0.5	97.699	97.501	97.436
0.1	97.439	97.431	97.428

s, spatial sampling ratio; σ, Poisson's ratio; p, stability parameter.

for example, $\beta = 300$ m/sec and travel distance of 10,000 m that are reasonable values in large sedimentary basins or valleys. Then, the delays in the S-wave arrival caused by the grid dispersion are 0.337 sec and 0.168 sec for the sampling ratio $s = 1/5$ and $s = 1/6$, respectively.

While there is practically no grid dispersion for the Poisson's ratio $\sigma = 0.495$ for the sampling ratios $s < 0.4$, $\alpha^{\mathrm{grid}}/\alpha > 1$ at all directions of propagation for the stability parameter $p = 1.0$ and Poisson's ratio $\sigma = 0.25$. The latter case means that the grid dispersion causes unphysically earlier P-wave arrivals. If necessary, and given relatively low sensitivity of $\beta^{\mathrm{grid}}/\beta$ to the stability parameter p, the earlier arrivals can be prevented by taking p as low as 0.5, i.e., by using half-value of the maximum possible time step Δt.

Figure 2(b) shows dispersion curves of the P-wave group velocity for three values of the Poisson's ratio σ and three values of the stability parameter p. Analogously, Figure 3(b) shows dispersion curves of the S-wave group velocity. What was said about the phase-velocity grid dispersion with respect to the Poisson's ratio σ and stability parameter p is qualitatively also true about the group-velocity grid dispersion. An important difference is considerably larger grid-dispersion anisotropy. Table 2 shows minimum $\beta^{\mathrm{grid}}_{\mathrm{group}}$ in percentage of β for two values of the sampling ratio s, $s = 1/5$ and $s = 1/6$, three values of the Poisson's ratio σ and three values of the stability parameter p. It is clear from Table 2 that for $s = 1/5$ and $s = 1/6$, $\beta^{\mathrm{grid}}_{\mathrm{group}}$ can differ from the actual velocity β as much as, approximately, 5% and 2.5%, respectively. Considering again the example with $\beta = 300$ m/sec and travel distance of 10,000 m, the delays in the S-wave energy arrival caused by the grid dispersion are 1.754 sec and 0.877 sec for the sampling ratios $s = 1/5$ and $s = 1/6$, respectively.

It is clear that taking six grid spacings per minimum wavelength of the S wave, i.e., $s = 1/6$, is better than taking only five grid spacings.

Propagation in the Coordinate-Axis Plane

Figure 4 shows dispersion curves for the P and S waves propagating in different directions in the coordinate xz-plane for the Poisson's ratio $\sigma = 0.25$ and stability parameter $p = 1.0$. From the two shown sets of the dispersion curves and from analogous ones for other values of p and σ (not shown here) it follows that for given values of s, p, and σ, c^{grid}/c (where c is α or β) increases from the minimum at the direction of the coordinate axis (here, the x-axis; $\delta = 90°$, $\varphi = 0°$) up to the maximum at the direction of the plane diagonal (here, the xz-plane diagonal; $\delta = 45°$, $\varphi = 0°$).

Propagation in the Body-Diagonal Plane

Figure 5 shows dispersion curves for the P and S waves propagating in the body-diagonal plane (here, the vertical plane determined by angle $\varphi = 45°$) for the Poisson's ratio $\sigma = 0.25$ and stability parameter $p = 1.0$. From Figure 5 as well as other sets of the dispersion curves (not shown here) it follows that for given values of s, p, and σ, c^{grid}/c (where c is α or β) increases from the minimum at the direction of the coordinate axis (here, the z-axis; $\delta = 0°$) up to the maximum at the direction of the body diagonal (here, the diagonal determined by $\delta = 54.74°$ and $\varphi = 0°$), and then decreases down to the value at the direction of the coordinate-plane diagonal (here, the xy-diagonal; $\delta = 90°$, $\varphi = 45°$).

Propagation in Three Distinct Directions

There are three distinct directions of propagation in the considered regular rectangular spatial grid: along a coordinate axis, coordinate-plane diagonal, and body diagonal. Here we consider the x-axis ($\delta = 90°$, $\varphi = 0°$), the xz-plane diagonal ($\delta = 45°$, $\varphi = 0°$), and body diagonal determined by $\delta = 54.74°$ and $\varphi = 45°$. They are illustrated in Figure 1. Figure 6 shows dispersion curves for the P wave propa-

GRID DISPERSION, 4th-ORDER 3D DISPLACEMENT-STRESS

$\varphi = 0.0$
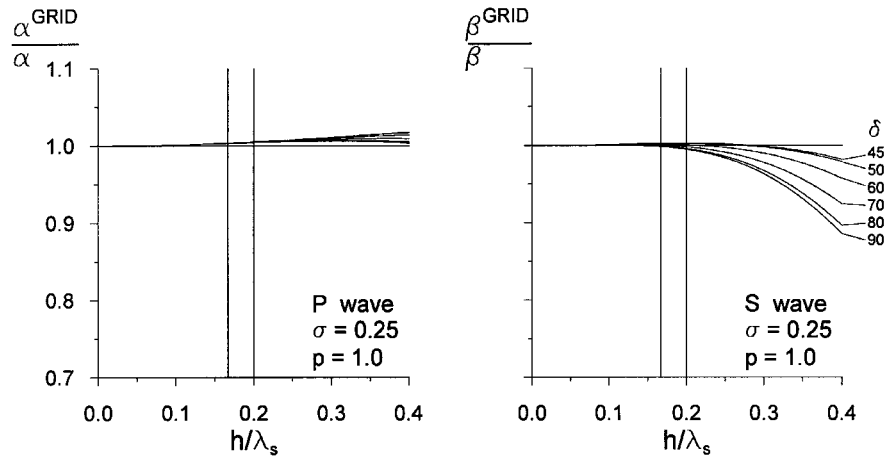
Figure 4. Grid dispersion curves for the *P* and *S* waves propagating in different directions in the coordinate *xz*-plane for the Poisson's ratio $\sigma = 0.25$ and stability parameter $p = 1.0$.

GRID DISPERSION, 4th-ORDER 3D DISPLACEMENT-STRESS

$\varphi = 45.0$
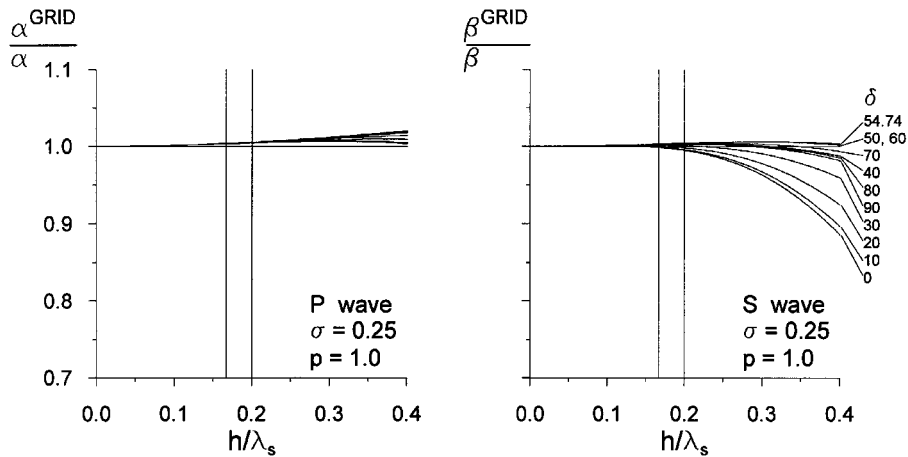
Figure 5. Grid dispersion curves for the *P* and *S* waves propagating in different directions in the body-diagonal plane for the Poisson's ratio $\sigma = 0.25$ and stability parameter $p = 1.0$.

gating in the three directions for three values of the Poisson's ratio σ and four values of the stability parameter p. Analogously, Figure 7 shows the dispersion curves for the *S* wave.

For given values of the spatial sampling ratio s, Poisson's ratio σ, and stability parameter p, c^{grid}/c (where c is α or β) exhibit a maximum at the direction of the body diagonal and minimum at the direction of the coordinate axis. In other words, grid dispersion is strongest for a wave propa-

gating along a coordinate axis and weakest for a wave propagating along a body diagonal.

Another interesting feature is that while $|\beta^{grid} - \beta|$ increases for $\sigma \to 0$ in the direction of a coordinate axis, it decreases in the direction of a body diagonal.

For a given type of wave, direction of propagation and value of the Poisson's ratio σ, c^{grid}/c decreases with decreasing value of the stability parameter p.

GRID DISPERSION FOR P WAVE, 4th-ORDER 3D DISPLACEMENT-STRESS
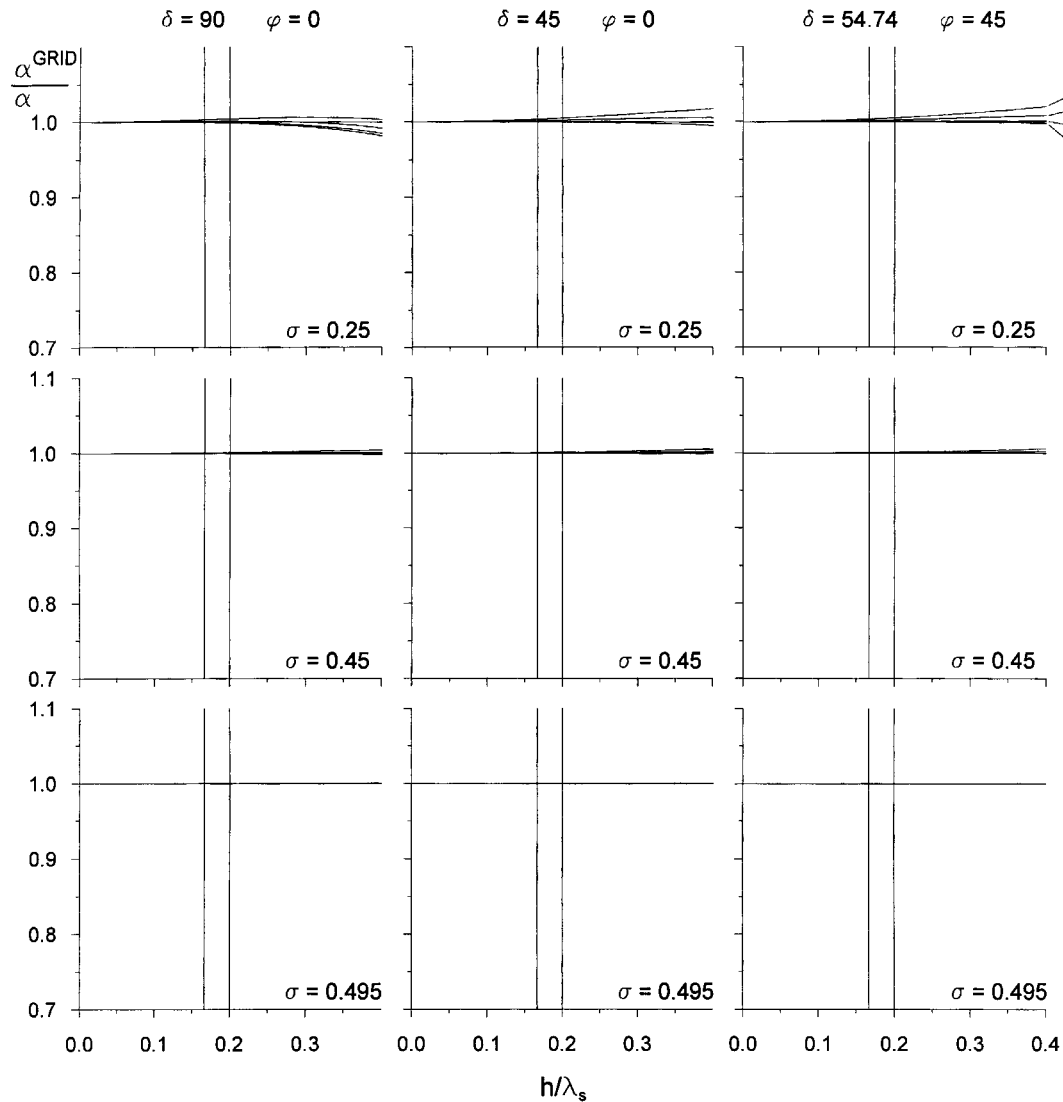
Figure 6.   Grid dispersion curves for the *P* wave propagating in the three distinct directions: along a coordinate axis, coordinate-plane diagonal, and body diagonal. Here we consider the *x*-axis ($\delta = 90°$, $\varphi = 0°$), the *xz*-plane diagonal ($\delta = 45°$, $\varphi = 0°$), and body diagonal ($\delta = 54.74°$, $\varphi = 45°$). The dispersion curves are shown for three values of the Poisson's ratio σ and four values of the stability parameter *p*.

For a given type of wave and direction of propagation, sensitivity of c^{grid}/c to the value of the stability parameter *p* considerably decreases as the value of the Poisson's ratio σ increases.

Since the grid dispersion is strongest in the direction of a coordinate axis, let us illustrate its effect on a plane *S* wave propagating in the direction of the x-axis ($\delta = 90°$, $\varphi = 0°$). Consider a medium with $\beta = 300$ m/sec and $\alpha = 1000$ m/sec, i.e., $\sigma = 0.4505$. Let the time function of the wave be Gabor signal

$$s(t) = \exp\{-[\omega_p\ (t - t_s)/\gamma_s]^2\}\ \cos[\omega_p\ (t - t_s) + \theta].$$

Here, $\omega_p = 2\pi f_p$, $t \in \langle 0, 2t_s\rangle$, $f_p = 0.5$ Hz is predominant frequency, $\gamma_s = 11$ controls the width of the signal, $\theta = \pi/2$ is a phase shift, and $t_s = 0.45\ \gamma_s/f_p$. The predominant frequency of 0.5 Hz is a typical one in recent seismic ground motion modeling. The amplitude spectrum of the signal is shown in Figure 8. The spectrum falls off by three orders of magnitude from its maximum at the frequency of 0.74 Hz.

In Figure 9 we show two cases. In the first one, a spatial

GRID DISPERSION FOR S WAVE, 4th-ORDER 3D DISPLACEMENT-STRESS
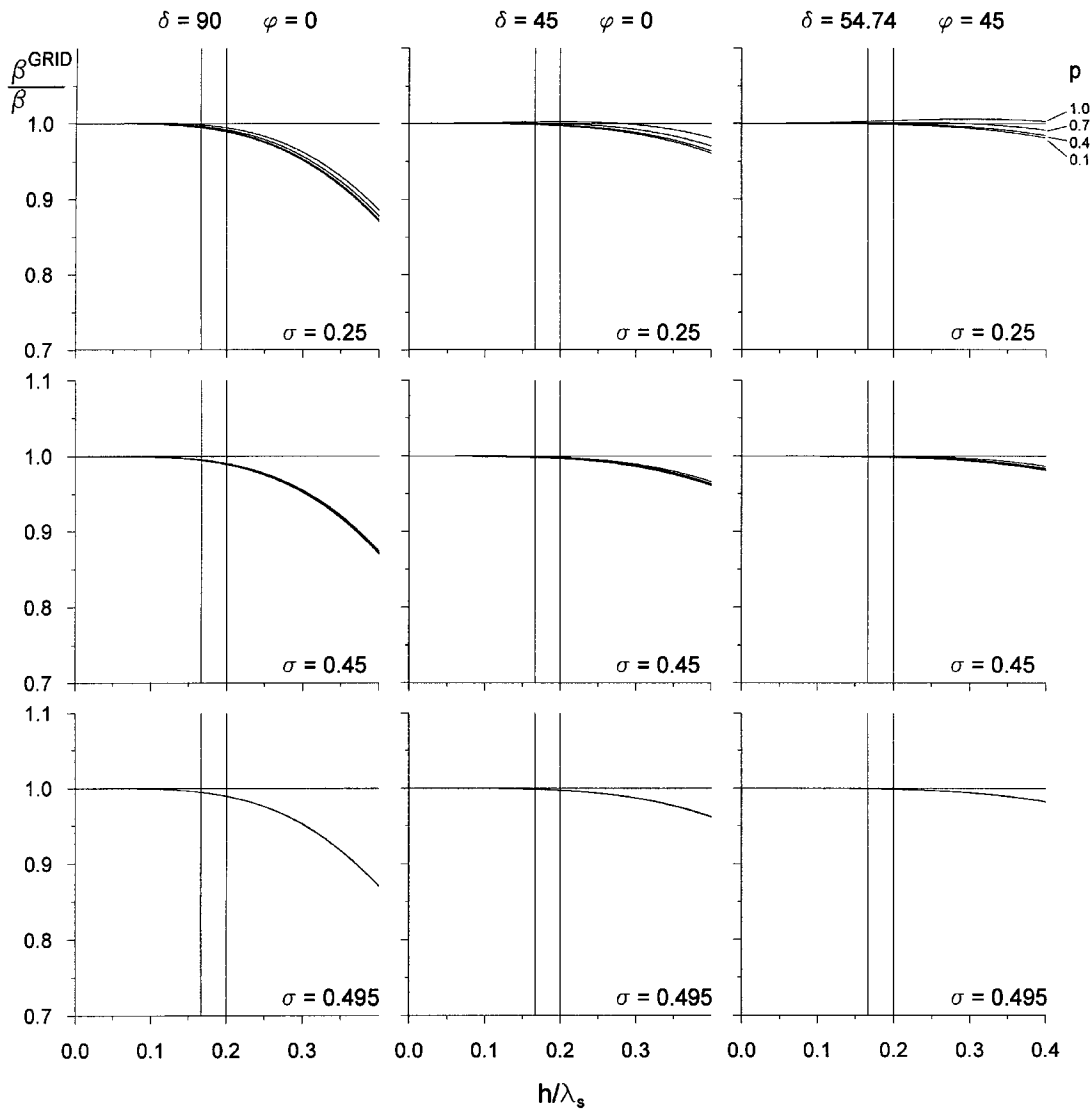
Figure 7.   The same as in Figure 6 but for the *S* wave.

sampling criterion is applied to a wavelength $\lambda_{0.5\ Hz}$ at the predominant frequency. Two numerical solutions, one for six and one for five grid spacings per $\lambda_{0.5\ Hz}$ are shown together with the exact solution (upper panel in Fig. 9). An effect of the grid phase-velocity dispersion is shown on the left-hand side (signals) while an effect of the grid group-velocity dispersion is shown on the right-hand side of the figure (envelopes). First, compare the numerical solution for five grid spacings per $\lambda_{0.5\ Hz}$ with the exact one. Both the signal and envelope of the numerical solution are distorted and delayed with respect to the exact solution. The delays of the maximum amplitudes of the signal and envelope are approximately 10% larger than delays simply predicted from the corresponding values of the grid phase and group veloc-

ities for a given travel distance. This is due to the effect of the spectral content of the Gabor signal at frequencies higher than the predominant frequency (see Fig. 8).

Compare now the two solutions with the numerical one for six grid spacings per $\lambda_{0.5\ Hz}$. We can see in Figure 9 that the delays of the maximum amplitudes of the signal and envelope (with respect to the exact solution) are approximately twice smaller compared with those for five grid spacings per $\lambda_{0.5\ Hz}$.

The lower part of Figure 9 compares the exact solution with two numerical ones for five and six grid spacings applied to $\lambda_{0.74\ Hz}$. As expected, delays due to the grid dispersion are much smaller compared with those in the earlier case.
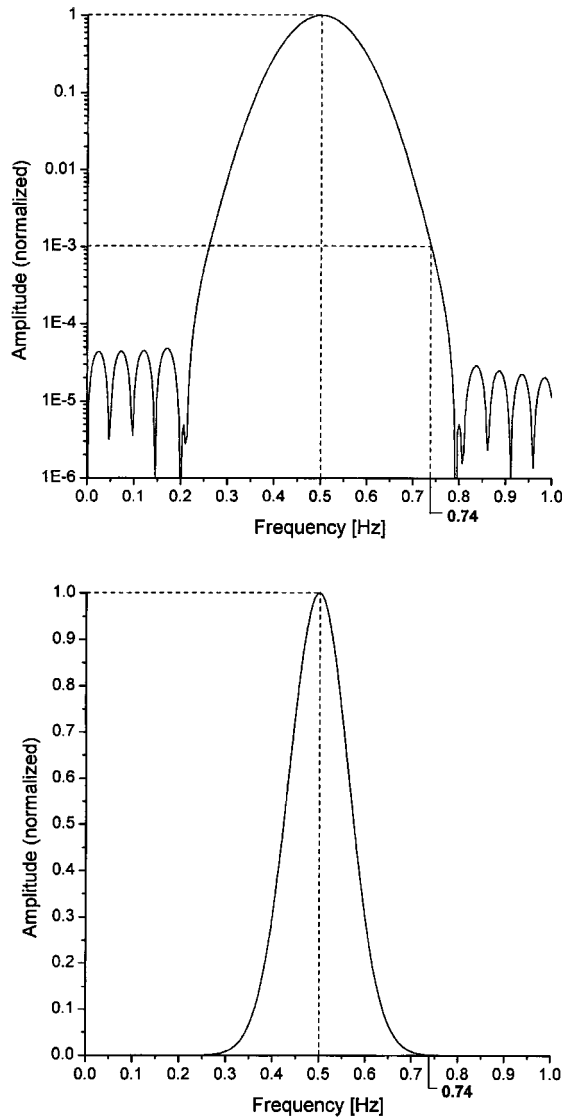
Figure 8. Amplitude Fourier spectrum of Gabor signal used in the example of an effect of the grid dispersion on a plane *S*-wave propagation.

An important fact in both cases is that using six grid spacings per wavelength instead of five grid spacings decreases delays in phase and energy arrivals approximately twice.

The example also indicates that it is not enough to apply a spatial sampling criterion to a wavelength corresponding to a predominant frequency if the spectral content at higher frequencies of a signal is non-negligible.

Comparison with the Second-Order Scheme

In order to compare grid dispersion in the fourth- and second-order schemes, we show in Figure 10 the *P*- and *S*-wave dispersion curves for both orders of approximation. Dispersion for the three distinct directions of propagation is

illustrated. It is very clear from Figure 10 that the difference between the two orders of approximation is significant. The second-order scheme models both the *P*- and *S*-wave propagation much worse than the fourth-order scheme.

There is one interesting exception in the second-order scheme. It is easy to see from equation (19) that for $\delta = 54.74°$ and $\varphi = 45°$ (body diagonal) and $p = 1.0$, $\alpha^{grid}/\alpha = 1$ for all values of the spatial sampling ratio s, i.e., there is no grid dispersion of the *P* wave propagating along the body diagonal at the stability limit. This is illustrated by a missing dispersion curve in the bottom left set of the curves in Figure 10. (The dispersion curve coincides with the horizontal line $\alpha^{grid}/\alpha = 1$.)

Another interesting feature of the grid dispersion in the second-order scheme is that $c^{grid}/c < 1$ (where c is α or β), i.e., there are no grid-dispersion related earlier arrivals.

Comparison with the 2D *P-SV* Case

Figure 11 illustrates the difference between the grid dispersion in the 3D and 2D *P-SV* cases. It follows from systematic investigation (figures not shown here) that sensitivity of the *P*- and *S*-wave grid dispersion to the stability parameter p is in the *P-SV* case larger than that in the 3D case regardless of the direction of propagation, value of the Poisson's ratio, and order of approximation. In this sense, the grid dispersion in the 2D *P-SV* case is worse than that in the 3D case.

Conclusions

We derived independent stability conditions for the *P* and *S* waves by exact separation of equations for the two types of waves.

Considering the *P*-wave stability condition as a joint stability condition, and the spatial sampling of the *S* wavelength at a given frequency as an argument in both dispersion relations, we consistently investigated the *P*- and *S*-wave grid dispersion.

Due to larger wavelength of the *P* wave, propagation of the *P* wave is modeled by the FD scheme much better than that of the *S* wave. Compared to the *P* wave, there is relatively considerable grid-dispersion anisotropy of the *S*-wave phase and mainly group velocity. The phase velocity β^{grid} does not differ not differ from the actual velocity β more than, approximately, 1% and 0.5% for the spatial sampling ratios $s = 1/5$ and $s = 1/6$, respectively. However, the group velocity β^{grid}_{group} can differ from β as much as 5% for the spatial sampling ratio $s = 1/5$ while it is 2.5% for $s = 1/6$. Therefore, we recommend to sample a minimum *S* wavelength by six grid spacings (instead of five that is prevailing practice).

Grid dispersion is strongest for a wave propagating along a coordinate axis and weakest for a wave propagating along a body diagonal.

From comparison with the grid dispersion in the second-order FD scheme it follows that the fourth-order scheme models wave propagation much better than the second-order
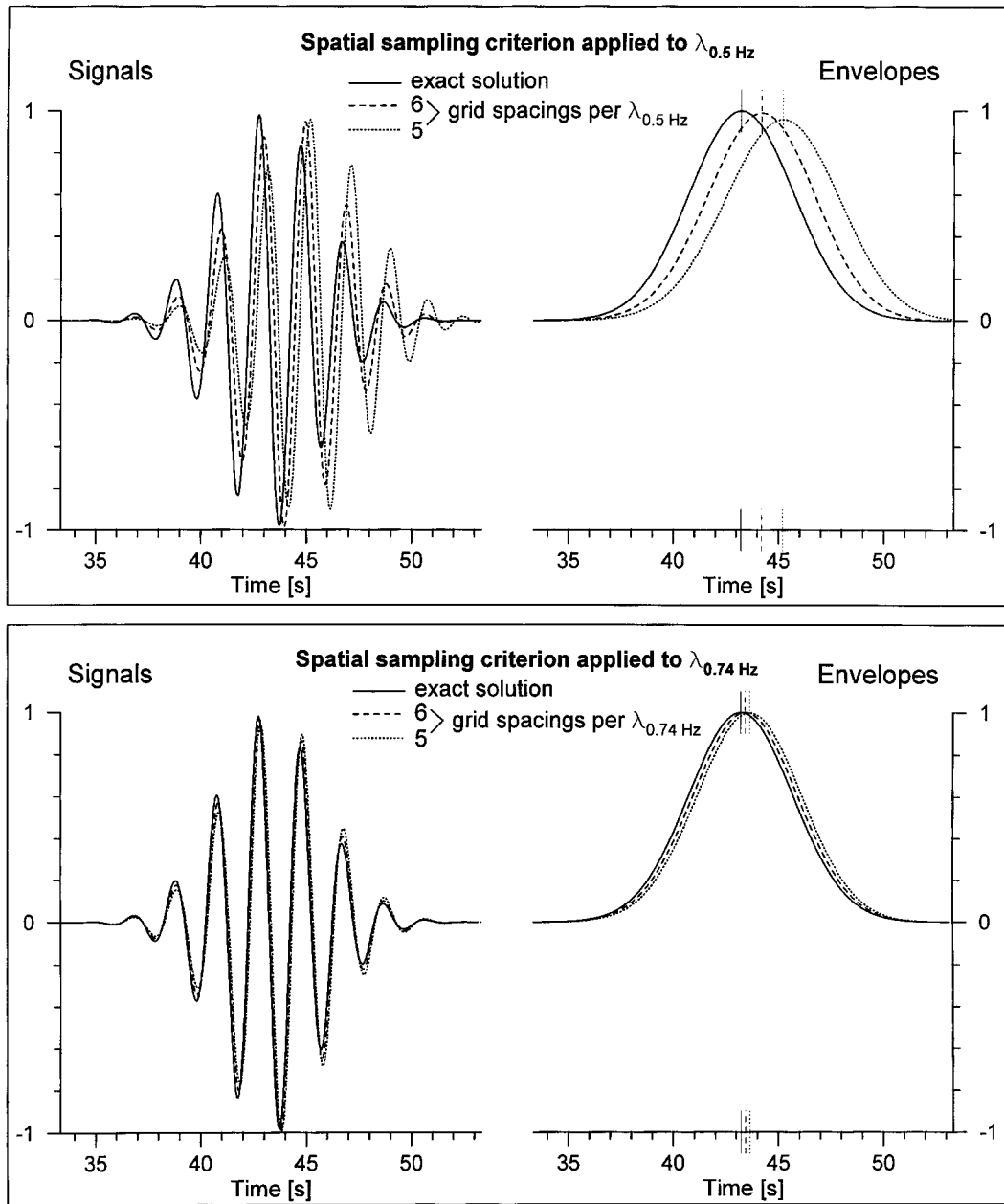
Figure 9. Example of an effect of the grid dispersion on a plane *S*-wave propagation in a grid in two cases. First, a spatial sampling criterion is applied to the wavelength at the predominant frequency of the signal ($\lambda_{0.5\,\text{Hz}} = 600$ m). Second, a spatial sampling criterion is applied to the wavelength at the frequency at which the amplitude spectrum falls off by three orders of magnitude from its maximum value ($\lambda_{0.74\,\text{Hz}} = 405$ m; see Fig. 8). All numerical solutions are compared with the exact one. Medium: $\beta = 300$ m/sec, $\alpha = 1000$ m/sec. Travel distance: 10,000 m. Direction of propagation: coordinate axis. Stability parameter: $p = 0.3$.

scheme. Moreover, grid dispersion in the second-order scheme for the sampling ratios $s = 1/10$ and $s = 1/12$ is larger than grid dispersion in the fourth-order scheme for $s = 1/5$ and $s = 1/6$, respectively.

Compared to the fourth-order 2D *P-SV* FD scheme, the grid dispersion in the fourth-order 3D FD scheme is consid-

erably less sensitive to a value of the stability parameter p.

Acknowledgments

Figure 10.   Comparison of the grid dispersion in the (a) fourth-order and (b) second-order FD schemes. The dispersion curves are shown for the *P* and *S* waves propagating in the three distinct directions (see Fig. 6) for the Poisson's ratio $\sigma = 0.25$ and four values of the stability parameter *p*.

References

Aoi, S., and H. Fujiwara (1999). 3-D finite-difference method using discontinuous grids, *Bull. Seism. Soc. Am.* **89,** 918–930.

Cotton, F., C. Berge, F. Lemeille, A. Pitarka, B. Lebrun, and M. Vallon (1998). Three-dimensional simulation of earthquakes in the Grenoble's basin, in *The Effects of Surface Geology on Seismic Motion,* K. Irikura, K. Kudo, H. Okada, and T. Sasatani (Editors), Vol. 2, Balkema, Rotterdam, 873–878.

Crase, E., C. Wideman, M. Noble, and A. Tarantola (1992). Nonlinear elastic waveform inversion of land seismic reflection data, *J. Geophys. Res.* **97,** 4685–4703.

Graves, R. W. (1993). Modeling three-dimensional site response effects in the Marina district basin, San Francisco, California, *Bull. Seism. Soc. Am.* **83,** 1042–1063.

Graves, R. W. (1996). Simulating seismic wave propagation in 3D elastic media using staggered-grid finite differences, *Bull. Seism. Soc. Am.* **86,** 1091–1106.

Graves, R. W., A. Pitarka, and P. G. Sommerville (1998). Ground-motion amplification in the Santa Monica area: effects of shallow basin-edge structure, *Bull. Seism. Soc. Am.* **88,** 1224–1242.

Hestholm, S., and B. Ruud (1998). 3-D finite-difference elastic wave modeling including surface topography, *Geophysics* **63,** 613–622.

Kristek, J., P. Moczo, K. Irikura, T. Iwata, and H. Sekiguchi (1999). The

GRID DISPERSION, 4th-ORDER DISPLACEMENT-STRESS

——— 3D   ------- PSV

$\sigma = 0.25$

Figure 11. Comparison of the grid dispersion in the (a) 3D and (b) 2D P-SV cases. The dispersion curves are shown for the *P* and *S* waves propagating in the direction of the *xz*-plane diagonal for the Poisson's ratio $\sigma = 0.25$ and four values of the stability parameter *p*.

1995 Kobe mainshock simulated by the 3D finite differences, in *The Effects of Surface Geology on Seismic Motion,* K. Irikura, K. Kudo, H. Okada, and T. Sasatani (Editors), Vol. 3, Balkema, Rotterdam, 1361–1368.

Levander, A. (1988). Fourth-order finite-difference *P-SV* seismograms, *Geophysics* **53,** 1425–1436.

Luo, Y., and G. Schuster (1990). Parsimonious staggered grid finite-differencing of the wave equation, *Geophys. Res. Lett.* **17,** 155–158.

Matsushima, S., H. Kawase, T. Sato, R. W. Graves, and P. G. Somerville (1998). 3D simulation of aftershocks of the Hyogo-ken Nanbu earthquake of 1995, in *The Effects of Surface Geology on Seismic Motion,* K. Irikura, K. Kudo, H. Okada, and T. Sasatani (Editors), Vol. 2, Balkema, Rotterdam, 1129–1136.

Moczo, P., J. Kristek, and E. Bystrický (in press). Efficiency and optimization of the 3D finite-difference modeling of seismic ground motion, *J. Comp. Acoustics.*

Ohminato, T., and B. A. Chouet (1997). A free-surface boundary condition for including 3D topography in the finite-difference method, *Bull. Seism. Soc. Am.* **87,** 494–515.

Olsen, K., and G. T. Schuster (1992). Seismic hazard analysis in Salt Lake Valley by finite-difference simulation of three dimensional elastic wave propagation, in *Scientific Excellence in High Performance Computing: The 1990 IBM Price Papers,* Vol. 1, Sec. 6, Baldwin Press, Athens, Georgia, 135–165.

Olsen, K. B., R. J. Archuleta, and J. R. Matarese (1995). Magnitude 7.75 earthquake on the San Andreas fault: three-dimensional ground motion in Los Angeles, *Science* **270,** 1628–1632.

Pitarka, A. (1999). 3D elastic finite-difference modeling of seismic motion using staggered grids with nonuniform spacing, *Bull. Seism. Soc. Am.* **89,** 54–68.

Pitarka, A., K. Irikura, and T. Iwata (1997). Modelling of ground motion in the Higashinada (Kobe) area for an aftershock of the 1995 January 17 Hyogo-ken Nanbu, Japan, earthquake. *Geophys. J. Int.* **131,** 231–239.

Pitarka, A., K. Irikura, T. Iwata, and H. Sekiguchi (1998). Three-dimensional simulation of the near-fault ground motion for the 1995 Hyogo-ken Nanbu (Kobe), Japan, earthquake, *Bull. Seism. Soc. Am.* **88,** 428–440.

Virieux, J. (1984). *SH*-wave propagation in heterogeneous media: velocity-stress finite-difference method, *Geophysics* **49,** 1933–1957.

Virieux, J. (1986). *P-SV* wave propagation in heterogeneous media: velocity-stress finite-difference method, *Geophysics* **51,** 889–901.

von Neumann, J. (1943). *Mathematische Grundlagen der Quantenmechanik,* Dover, New York.

Wald, D., and R. W. Graves (1998). The seismic response of the Los Angeles Basin, California, *Bull. Seism. Soc. Am.* **88,** 337–356.

Yomogida, K., and J. T. Etgen (1993). 3-D wave propagation in the Los Angeles basin for the Whittier-Narrows earthquake, *Bull. Seism. Soc. Am.* **83,** 1325–1344.

Geophysical Institute
Slovak Academy of Sciences
Dúbravská cesta 9
842 28 Bratislava, Slovak Republic
(P. M., J. K.)

Department of Mathematics
Engineering Faculty
Slovak Technical University
Nám. Slobody 17
812 31 Bratislava
Slovak Republic
(L. H.)

Appendix

3D Fourth-Order Displacement-Stress Staggered-Grid FD Scheme

$$
\begin{aligned}
U_{I,K+1/2,L+1/2}^{m+1} = {} & 2U_{I,K+1/2,L+1/2}^{m} - U_{I,K+1/2,L+1/2}^{m-1} + (\Delta^2 t/\rho_{I,K+1/2,L+1/2}^{U})\, F_{I,K+1/2,L+1/2}^{x,m} \\
& + \frac{\Delta^2 t}{h} \frac{1}{\rho_{I,K+1/2,L+1/2}^{U}} [a(T_{I+3/2,K+1/2,L+1/2}^{xx,m} - T_{I-3/2,K+1/2,L+1/2}^{xx,m}) \\
& + b(T_{I+1/2,K+1/2,L+1/2}^{xx,m} - T_{I-1/2,K+1/2,L+1/2}^{xx,m}) \\
& + a(T_{I,K+2,L+1/2}^{xy,m} - T_{I,K-1,L+1/2}^{xy,m}) \\
& + b\,(T_{I,K+1,L+1/2}^{xy,m} - T_{I,K,L+1/2}^{xy,m}) \\
& + a\,(T_{I,K+1/2,L+2}^{xz,m} - T_{I,K+1/2,L-1}^{xz,m}) \\
& + b\,(T_{I,K+1/2,L+1}^{xz,m} - T_{I,K+1/2,L}^{xz,m})]
\end{aligned}
$$

$$
\begin{aligned}
V_{I+1/2,K,L+1/2}^{m+1} = {} & 2V_{I+1/2,K,L+1/2}^{m} - V_{I+1/2,K,L+1/2}^{m-1} + (\Delta^2 t/\rho_{I+1/2,K,L+1/2}^{V})\, F_{I+1/2,K,L+1/2}^{y,m} \\
& + \frac{\Delta^2 t}{h} \frac{1}{\rho_{I+1/2,K,L+1/2}^{V}} [a(T_{I+2,K,L+1/2}^{xy,m} - T_{I-1,K,L+1/2}^{xy,m}) \\
& + b(T_{I+1,K,L+1/2}^{xy,m} - T_{I,K,L+1/2}^{xy,m}) \\
& + a\,(T_{I+1/2,K+3/2,L+1/2}^{yy,m} - T_{I+1/2,K-3/2,L+1/2}^{yy,m}) \\
& + b\,(T_{I+1/2,K+1/2,L+1/2}^{yy,m} - T_{I+1/2,K-1/2,L+1/2}^{yy,m}) \\
& + a\,(T_{I+1/2,K,L+2}^{yz,m} - T_{I+1/2,K,L-1}^{yz,m}) \\
& + b\,(T_{I+1/2,K,L+1}^{yz,m} - T_{I+1/2,K,L}^{yz,m})]
\end{aligned}
$$

$$
\begin{aligned}
W_{I+1/2,K+1/2,L}^{m+1} = {} & 2W_{I+1/2,K+1/2,L}^{m} - W_{I+1/2,K+1/2,L}^{m-1} + (\Delta^2 t/\rho_{I+1/2,K+1/2,L}^{W})\, F_{I+1/2,K+1/2,L}^{z,m} \\
& + \frac{\Delta^2 t}{h} \frac{1}{\rho_{I+1/2,K+1/2,L}^{W}} [a(T_{I+2,K+1/2,L}^{xz,m} - T_{I-1,K+1/2,L}^{xz,m}) \\
& + b\,(T_{I+1,K+1/2,L}^{xz,m} - T_{I,K+1/2,L}^{xz,m}) \\
& + a\,(T_{I+1/2,K+2,L}^{yz,m} - T_{I+1/2,K-1,L}^{yz,m}) \\
& + b\,(T_{I+1/2,K+1,L}^{yz,m} - T_{I+1/2,K,L}^{yz,m}) \\
& + a\,(T_{I+1/2,K+1/2,L+3/2}^{zz,m} - T_{I+1/2,K+1/2,L-3/2}^{zz,m}) \\
& + b\,(T_{I+1/2,K+1/2,L+1/2}^{zz,m} - T_{I+1/2,K+1/2,L-1/2}^{zz,m})]
\end{aligned}
$$

$$
\begin{aligned}
T_{I+1/2,K+1/2,L+1/2}^{xx,m} = {} & \frac{1}{h} \{ (\lambda + 2\mu)_{I+1/2,K+1/2,L+1/2} [a(U_{I+2,K+1/2,L+1/2}^{m} - U_{I-1,K+1/2,L+1/2}^{m}) \\
& + b\,(U_{I+1,K+1/2,L+1/2}^{m} - U_{I,K+1/2,L+1/2}^{m})] \\
& + \lambda_{I+1/2,K+1/2,L+1/2} [a(V_{I+1/2,K+2,L+1/2}^{m} - V_{I+1/2,K-1,I+1/2}^{m}) \\
& + b\,(V_{I+1/2,K+1,L+1/2}^{m} - V_{I+1/2,K,L+1/2}^{m}) \\
& + a\,(W_{I+1/2,K+1/2,L+2}^{m} - W_{I+1/2,K+1/2,L-1}^{m}) \\
& + b\,(W_{I+1/2,K+1/2,L+1}^{m} - W_{I+1/2,K+1/2,L}^{m})]\}
\end{aligned}
$$

$$
\begin{aligned}
T_{I+1/2,K+1/2,L+1/2}^{yy,m} = {} & \frac{1}{h} \{ \lambda_{I+1/2,K+1/2,L+1/2} [a(U_{I+2,K+1/2,L+1/2}^{m} - U_{I-1,K+1/2,L+1/2}^{m}) \\
& + b\,(U_{I+1,K+1/2,L+1/2}^{m} - U_{I,K+1/2,L+1/2}^{m})] \\
& + (\lambda + 2\mu)_{I+1/2,K+1/2,L+1/2} [a\,(V_{I+1/2,K+2,L+1/2}^{m} - V_{I+1/2,K-1,L+1/2}^{m}) \\
& + b\,(V_{I+1/2,K+1,L+1/2}^{m} - V_{I+1/2,K,L+1/2}^{m})] \\
& + \lambda_{I+1/2,K+1/2,L+1/2} [a\,(W_{I+1/2,K+1/2,L+2}^{m} - W_{I+1/2,K+1/2,L-1}^{m}) \\
& + b\,(W_{I+1/2,K+1/2,L+1}^{m} - W_{I+1/2,K+1/2,L}^{m})]\}
\end{aligned}
$$

$$
\begin{aligned}
T_{I+1/2,K+1/2,L+1/2}^{zz,m} = {} & \frac{1}{h} \{ \lambda_{I+1/2,K+1/2,L+1/2} [a\,(U_{I+2,K+1/2,L+1/2}^{m} - U_{I-1,K+1/2,L+1/2}^{m}) \\
& + b(U_{I+1,K+1/2,L+1/2}^{m} - U_{I,K+1/2,L+1/2}^{m}) \\
& + a\,(V_{I+1/2,K+2,L+1/2}^{m} - V_{I+1/2,K-1,L+1/2}^{m}) \\
& + b\,(V_{I+1/2,K+1,L+1/2}^{m} - V_{I+1/2,K,L+1/2}^{m})] \\
& + (\lambda + 2\mu)_{I+1/2,K+1/2,L+1/2} [a\,(W_{I+1/2,K+1/2,L+2}^{m} - W_{I+1/2,K+1/2,L-1}^{m}) \\
& + b(W_{I+1/2,K+1/2,L+1}^{m} - W_{I+1/2,K+1/2,L}^{m})]\}
\end{aligned}
$$

$$T_{I,K,L+1/2}^{xy,m} = \frac{1}{h} \mu_{I,K,L+1/2} \, [a \, (U_{I,K+3/2,L+1/2}^m - U_{I,K-3/2,L+1/2}^m)$$
$$+ \, b \, (U_{I,K+1/2,L+1/2}^m - U_{I,K-1/2,L+1/2}^m)$$
$$+ \, a \, (V_{I+3/2,K,L+1/2}^m - V_{I-3/2,K,L+1/2}^m)$$
$$+ \, b \, (V_{I+1/2,K,L+1/2}^m - V_{I-1/2,K,L+1/2}^m)]$$

$$T_{I,K+1/2,L}^{xz,m} = \frac{1}{h} \mu_{I,K+1/2,L} \, [a \, (U_{I,K+1/2,L+3/2}^m - U_{I,K+1/2,L-3/2}^m)$$
$$+ \, b \, (U_{I,K+1/2,L+1/2}^m - U_{I,K+1/2,L-1/2}^m)$$
$$+ \, a \, (W_{I+3/2,K+1/2,L}^m - W_{I-3/2,K+1/2,L}^m)$$
$$+ \, b \, (W_{I+1/2,K+1/2,L}^m - W_{I-1/2,K+1/2,L}^m)]$$

$$T_{I+1/2,K,L}^{yz,m} = \frac{1}{h} \mu_{I+1/2,K,L} \, [a(V_{I+1/2,K,L+3/2}^m - V_{I+1/2,K,L-3/2}^m)$$
$$+ \, b \, (V_{I+1/2,K,L+1/2}^m - V_{I+1/2,K,L-1/2}^m)$$
$$+ \, a \, (W_{I+1/2,K+3/2,L}^m - W_{I+1/2,K-3/2,L}^m)$$
$$+ \, b \, (W_{I+1/2,K+1/2,L}^m - W_{I+1/2,K-1/2,L}^m)]$$

The second-order scheme is obtained from the fourth-order scheme by inserting $a = 0$ and $b = 1$.

Grid-Dispersion Relations for the 2D *P-SV* Fourth-Order Displacement-Stress Staggered-Grid FD Scheme

$$\frac{\alpha^{\text{grid}}}{\alpha} = q \, \frac{\sqrt{2}}{\pi} \, \frac{r}{p \cdot s} \, \arcsin \left(\frac{1}{q\sqrt{2}} \, p \, F_a \right)$$

$$\frac{\beta^{\text{grid}}}{\beta} = q \, \frac{\sqrt{2}}{\pi} \, \frac{r}{p \cdot s} \, \arcsin \left(\frac{1}{q\sqrt{2}} \, \frac{p}{r} \, F_\beta \right)$$

where

$$q = \frac{7}{6}$$

$$F_\eta = \{[a \, \sin \, (3\pi\varsigma \, \sin \, \delta) + b \, \sin \, (\pi\varsigma \, \sin \, \delta)]^2$$
$$+ \, [a \, \sin \, (3\pi\varsigma \, \cos \, \delta) + b \, \sin \, (\pi\varsigma \, \cos \, \delta)]^2\}^{1/2}$$

and

$$\varsigma = \frac{s}{r} \quad \text{if} \quad \eta = \alpha$$

or

$$\varsigma = s \quad \text{if} \quad \eta = \beta.$$

The stability parameter p is defined as

$$p = \sqrt{2} \, \frac{7}{6} \, \frac{\Delta t}{h} \, \alpha, \qquad p \le 1.$$

The grid-dispersion relations for the second-order scheme are obtained by inserting $a = 0$, $b = 1$, and $q = 1$. The stability parameter p in the second-order scheme is defined as

$$p = \sqrt{2} \, \frac{\Delta t}{h} \, \alpha, \qquad p \le 1.$$